Geomechanics and Engineering, *Vol. 22, No. 6 (2020) 497-507*
DOI: https://doi.org/10.12989/gae.2020.22.6.497

Effect of new tunnel construction on structural performance of existing tunnel lining

Chungsik Yoo*[1] and Shuaishuai Cui[2]

[1]School of Civil, Architectural Engineering and Landscape Architecture, Sungkyunkwan University, 2066 Seboo-ro, Jangan-gu, Suwon, Kyounggi-do 16419, Republic of Korea
[2]School of Civil Engineering, Shandong University, No. 17923, Jingshi Road, Jinan, Shandong Province, China

(Received March 10, 2020, Revised July 11, 2020, Accepted August 17, 2020)

Abstract. This paper presents the results of a three-dimensional numerical investigation into the effect of new tunnel construction on structural performance of existing tunnel lining. A three-dimensional finite difference model, capable of modelling the tunnel construction process, was adopted to perform a parametric study on the spatial variation of new tunnel location with respect to the existing tunnel with emphasis on the plan crossing angle of the new tunnel with respect to the existing tunnel and the vertical elevation of the new tunnel with respect to the existing one. The results of the analyses were arranged so that the effect of new tunnel construction on the lining member forces and stresses of the existing tunnel can be identified. The results indicate that when a new tunnel underpasses an existing tunnel, the new tunnel construction imposes greater impact on the existing tunnel lining when the two tunnels cross at an acute angle. Also shown are that the critical plan crossing angle of the new tunnel that would impose greater impact on the existing tunnel depends on the relative vertical location of the new tunnel with respect to the existing one, and that the overpassing new tunnel construction scenario is more critical than the underpassing scenario in view of the existing tunnel lining stability. Practical implications of the findings are discussed.

Keywords: conventional tunneling; crossing tunnel interaction; underpassing tunnel; overpassing tunnel; finite-difference analysis; lining member forces

1. Introduction

When constructing an urban subway tunnel, there are many instances where a new tunnel is constructed under or over an existing subway line (Choi and Lee 2010, Talebinejad *et al.* 2013). In such cases, the structural impact of the new tunnel construction on the existing tunnel should be strictly controlled as specifications require (Hansmire *et al.* 2004, Byun *et al.* 2006, Lai *et al.* 2015). As construction of a new tunnel, either under- or overpassing, may impose structural impact on the existing tunnel structure, permanent lining in particular, such projects are often challenging and require high precision control (Ng *et al.* 2013, Zhang *et al.* 2015).

In the past there have been many studies on the subject of interaction between new tunnel construction and an existing tunnel. These studies mainly focused on the development of construction technology together with the prediction and control of ground settlement, based on analytical study, field measured data, numerical simulation, and physical modeling. For example, Cooper *et al.* (2002) developed an empirical method for estimating the settlement trough caused by the second of twin tunnels based on measured field data, which can be used as a preliminary predictive tool. Later, Yoo and Song (2006) conducted a study that considered a number of construction scenarios in terms of relative location of a new tunnel to an existing tunnel using 2D and 3D finite element models. Later, Zhang and Huang (2014) performed deformation analyses of the existing subway tunnels induced by an earth pressure balance (EPB) shield during the construction of overlapping and underlapping tunnels crossing at oblique angles. Most recently, Boonyarak and Ng (2015) carried out centrifuge tests to investigate the effects of construction sequence on crossing–tunnel interaction. In their study, the existing tunnel was found to be vertically compressed when the new tunnel was excavated underneath, but vertically elongated when the new tunnel was advanced on top of the existing tunnel. Nawel and Salah (2015) reported results of a numerical study on two parallel tunnel interaction using three-dimensional finite element method. More recently, Eskandari *et al.* (2018) analyzed the measured data during an EPB tunneling and reported the impact of EPB pressure on surface settlement and face displacement in intersection of triple tunnels at Mashhad metro. The influence of excavation phase shift on the twin-tunnel interaction was also investigated by Djelloul *et al.* (2018) using 2D numerical modeling. They reported, among other things, that the structural lining forces induced in the first tunnel through various phases are considerably affected by the second tunnel construction process.

It is certain that aforementioned studies have identified

*Corresponding author, Professor
E-mail: csyoo@skku.edu

ISSN: 2005-307X (Print), 2092-6219 (Online)

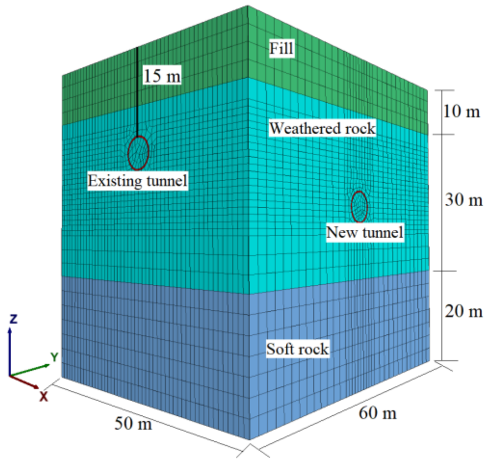

(a) Geometry of finite-difference model

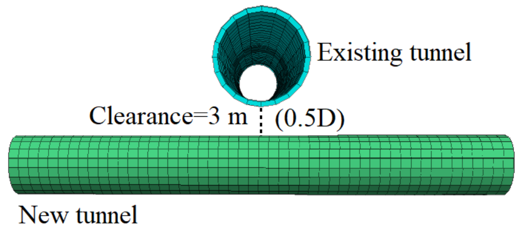

(b) Clearance definition

Fig. 1 Schematic view of tunneling condition considered (underpassing)

Table 1 Geotechnical properties of ground layers

Material	E (MPa)	ν	c' (kPa)	ϕ' (°)	γ (kN/m^3)
Fill	20	0.32	21	29	20
Weathered rock	290	0.30	70	32	22
Soft rock	910	0.27	440	37	24

E=Young's modulus; ν=Poisson's ratio; c'=cohesion; ϕ'=internal friction angle; γ=unit weight

the important governing mechanism of the effect of new tunnel construction on an existing tunnel. Most of the previous studies, however, adopted rather ideal and simplified tunneling situations, which in turn limits the applicability of their findings to real life tunneling situations. In this study, a three-dimensional numerical investigation into the effect of new tunnel construction (underpassing and overpassing) on an existing tunnel was carried out aiming at supplementing additional data to the findings from the previous studies. A series of hypothetical tunneling situations were first developed to cover a wide range of spatial variations of new tunnel construction cases in terms of the plan orientation of the new tunnel with respect to the existing tunnel axis. The parametric study was conducted using a 3D finite-difference model using FLAC3D (Itasca Consulting Group, 2017), which can realistically model the non-linear material behavior of the ground and the tunneling sequence. The following sections present the tunneling conditions, the 3D finite-difference model, and the practical implications of the findings.

2. Tunneling conditions considered

2.1 Tunneling and ground conditions

Fig. 1 shows a typical tunneling condition considered in this study. As shown, this study considered tunneling cases where a 6 m diameter (D=6 m) circular tunnel is constructed by the conventional tunneling method either under (underpassing) or over (overpassing) an existing tunnel of the same diameter. The clearance between the two tunnels is kept constant at 3 m, i.e., 0.5D to represent rather severe tunneling cases with various plan orientations of the new tunnel with respect to that of the existing tunnel. For the underpassing tunneling situations, the cover depth of the existing tunnel was selected as 2.5D (i.e., C=15 m). For the overpassing cases, on the other hand, the positions of the two tunnels were switched, giving the cover depths of the new and existing tunnels as 2.5D and 4.0D, respectively. Note that the tunnel cover depths of the underpassing and overpassing tunnels were not the same as the cover depth of the existing tunnel was kept constant for those cases. Despite the inherent difference in the cover depths of the two, the direct comparison between the underpassing and overpassing cases is thought to identify key differences in the response of the existing tunnel to each tunneling case.

The existing tunnel was assumed to be supported by a 300 mm thick permanent unreinforced concrete lining. Furthermore, the new tunnel was assumed to be excavated in full face with a 300 mm thick shotcrete layer as a primary support. Although system rock bolts are usually adopted in this type of tunneling situation, no rock bolts were considered for simplicity.

The ground considered in this study includes a 10 m thick fill underlain by a 30 m thick weathered granite rock layer of Grade *III* as per the engineering classification of rock (Waltham 1994) having RMR values ranging from 30 to 40, in which the new and existing tunnels are located. Following this is a soft granitic rock layer of Grade II, having RMR values ranging from 50 to 60. No groundwater table was considered in this investigation. The geotechnical properties of the different layers are summarized in Table 1.

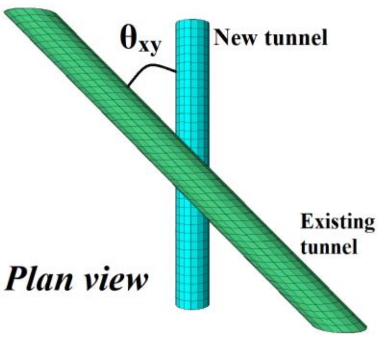

Fig. 2 Definition of plan crossing angle (θ_{xy})

2.2 Construction scenarios considered

Various new tunnel construction scenarios were considered in this study. For the underpassing cases, an emphasis was placed on the effect of orientation of the new tunnel with respect to the existing tunnel. The orientation of the new tunnel was expressed in terms of plan crossing angle (θ_{xy}) between the new and existing tunnels as shown in Fig. 2, which were varied from 0 to 90 degrees to grasp complete interaction mechanism between the two tunnels. Limited overpassing cases with plan crossing angles of $\theta_{xy} = 0°$ and $90°$ were additionally considered in order to examine the effect of vertical elevation of the new tunnel with respect to the existing tunnel.

3. Three-dimensional finite difference analysis

Three-dimensional finite difference models capable of simulating the sequential tunneling process were adopted in order to realistically capture the three-dimensional tunnel interaction. A particular attention was paid to the modelling of the new tunnel construction sequence to allow for realistic simulation of the new and existing tunnel interaction. Details of the three-dimensional model are given under subsequent paragraphs.

3.1 3D finite differnce model

A typical finite-difference model adopted in this study is shown in Fig. 1, which consists of approximately 64,000 elements with over 69,000 nodes. In order to define the model, the lateral boundaries were placed at locations with sufficient distance to eliminate possible boundary effects; i.e., 5.0D from the existing tunnel center for the lateral vertical boundaries and 8.3D from the tunnel portal for the longitudinal vertical boundary, and the bottom boundary at 5.0D from the lower tunnel invert (Fig. 1). In terms of the displacement boundary condition, roller boundaries were placed on the vertical faces of the mesh, i.e., $u_x = u_y = 0$, while a fixed boundary condition was assumed at the bottom boundary considering the rigid rock layer.

In dicretization, the ground was modeled using solid elements, while three-dimensional conventional shell elements were used for the shotcrete and permanent linings. With regard to the constitutive modeling, the ground was assumed to be an elasto-plastic material conforming to the Mohr-Coulomb failure criterion, together with the non-associated flow rule proposed by Davis (1968), while the shotcrete and permanent linings were assumed to behave in a linear elastic manner. The time dependency of the strength and stiffness of the shotcrete lining after installation was not explicitly modeled in the analysis; instead, an average value of Young’s modulus of 10 GPa, representing the green and hard shotcrete conditions reported in the literature Queiroz *et al.* (2006), was employed. The Young’s modulus of the permanent lining was also taken as 15 GPa, considering the possible material degradation over time while the unit weight of 25 kN/m^3 and Poisson’s ratio of 0.3 were adopted for both the shotcrete and permanent linings.

3.2 Tunnel construction modeling

After creating the initial stress condition of the ground with appropriate boundary conditions, assuming the lateral stress coefficient of $K_0 = 0.43$, the existing tunnel was created by simulating the step by step tunneling process. The tunneling process, consisting of a series of full-face excavation with an advance length of 2 m and 150 mm thick shotcrete lining installation, was closely followed by removing and adding corresponding elements at designated steps. After completion of the excavation of the existing tunnel, a 300 mm thick unreinforced concrete lining was additionally installed as a permanent lining. The new tunnel was also excavated in full-face with an advance length of 2 m, followed by 300 mm thick shotcrete lining installation after each round of excavation.

4. Results and discussion

Results of the 3D finite-difference analyses were examined so that the interaction mechanism between the new and the existing tunnels can be identified using the new tunnel construction induced member forces and stresses in the permanent lining of the existing tunnel. Lining forces and stresses presented in the subsequent sections thus represent for those developed in the existing tunnel lining caused by the new tunnel construction unless otherwise indicated. The positive member forces are designated as shown in Fig. 3.

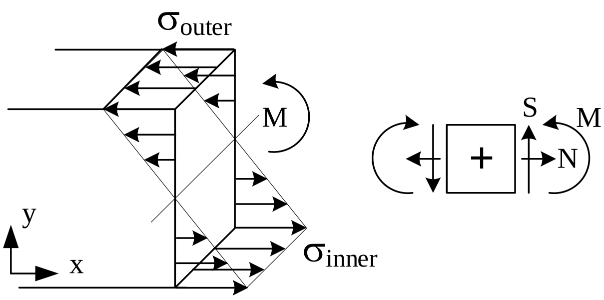

Fig. 3 Sign convention adopted for lining member forces (positive shown)

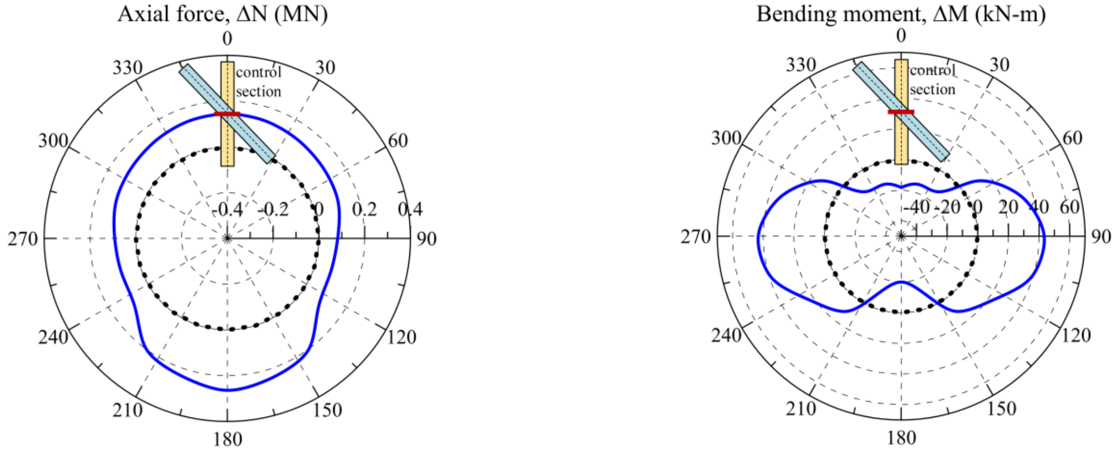

(a) Axial force (ΔN) (b) Bending moment (ΔM)

Fig. 4 New tunnel construction induced existing tunnel lining member forces (underpassing, $\theta_{xy} = 90°$)

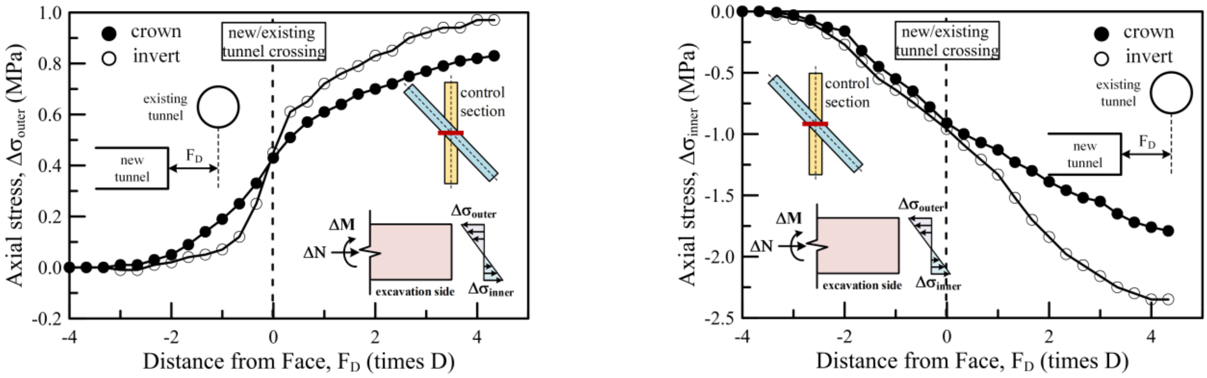

(a) Axial stress ($\Delta\sigma_{outer}$) (b) Axal stress ($\Delta\sigma_{inner}$)

Fig. 5 Evolution of $\Delta\sigma_{outer}$ and $\Delta\sigma_{inner}$ with new tunnel advance (underpassing, $\theta_{xy} = 90°$)

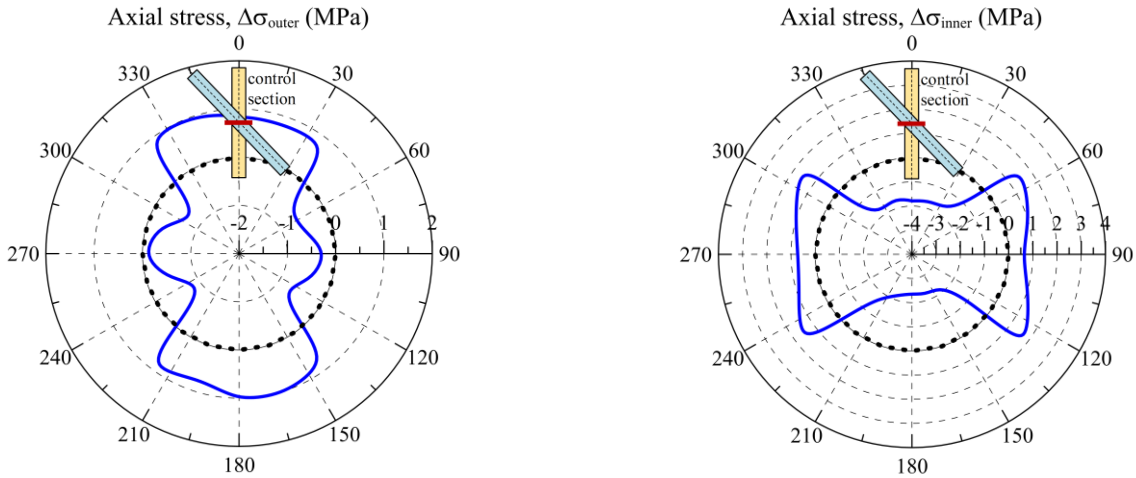

(a) Outer surface axial stress ($\Delta\sigma_{outer}$) (b) Inner surface axial stress ($\Delta\sigma_{inner}$)

Fig. 6 New tunnel construction induced existing tunnel lining stresses (underpassing, $\theta_{xy} = 90°$)

4.1 General mechanism of new tunnel impact on existing tunnel

Fig. 4 shows the new tunnel-induced axial force (ΔN) and bending moment (ΔM) at the control section (colored in red) of the existing tunnel lining for the underpassing case of which the new and the existing tunnels cross at right angle, i.e., $\theta_{xy} = 90°$. As shown, due to the symmetry about the vertical axis of the new tunnel, the shape of the ΔN and ΔM profiles appears to be almost symmetrical about the vertical axis showing a maximum axial force of $\Delta N_{max} \approx 0.26\ MN$ and bending moment of $\Delta M_{max} \approx 42\ kN \cdot m$ at the invert and the spring line, respectively. Note that the bending moments at the crown and invert

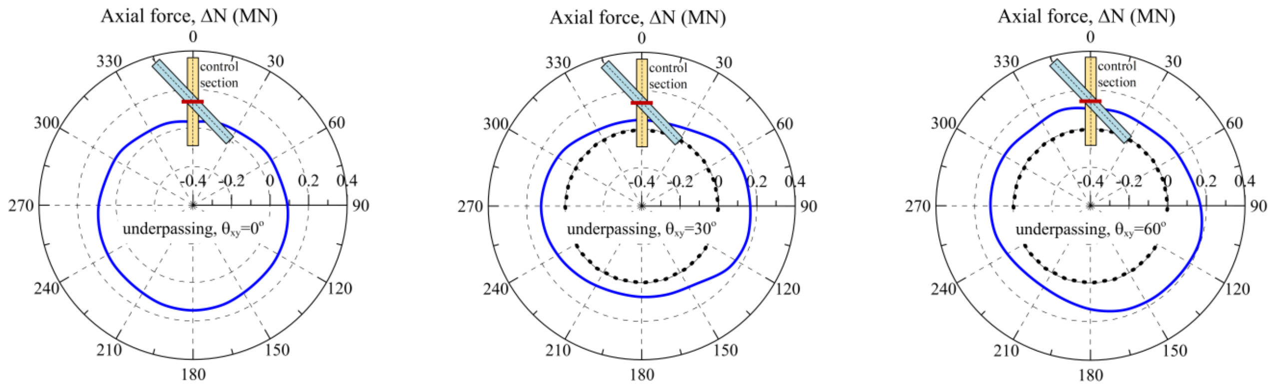

(a) $\theta_{xy} = 0°$ (b) $\theta_{xy} = 30°$ (c) $\theta_{xy} = 60°$

Fig. 7 Effect of plan crossing angle on new tunnel induced existing tunnel lining axial force (underpassing)

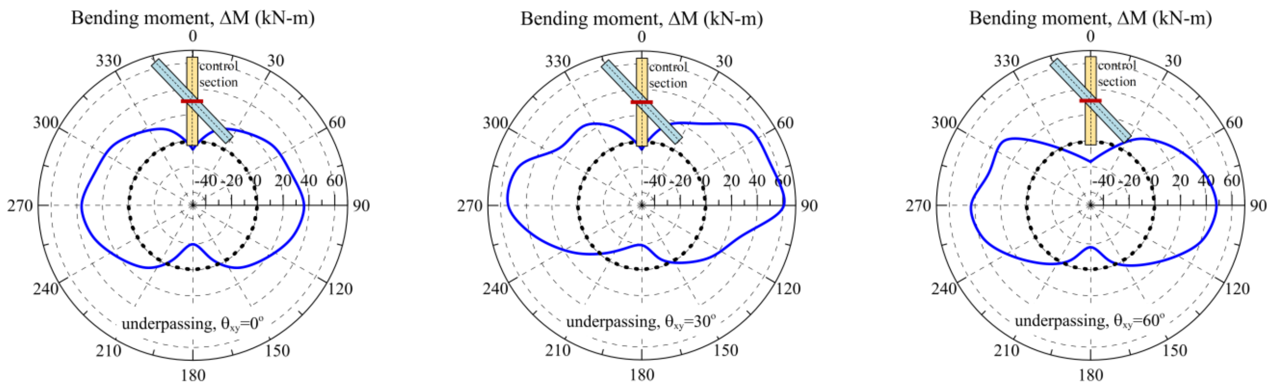

(a) $\theta_{xy} = 0°$ (b) $\theta_{xy} = 30°$ (c) $\theta_{xy} = 60°$

Fig. 8 Effect of plan crossing angle on new tunnel induced existing tunnel lining bending moment (underpassing)

locations are negative (convex) while those at the spring lines are positive (concave) with axial forces in tension prevailing all around. The ovalized deformation pattern of the existing tunnel lining caused by the new tunnel construction is responsible for such trend, although not shown here.

The progressive development of the lining stresses normal to the cross section, imposed by the new tunnel excavation, is shown in Fig. 5 using $\Delta\sigma_{outer}$ and $\Delta\sigma_{inner}$ at two locations, i.e., crown and invert. Note that $\Delta\sigma_{outer}$ and $\Delta\sigma_{inner}$ are the normal stresses on the outer and inner sides, respectively, as defined in Fig. 3, calculated from the ΔN and ΔM. As shown, $\Delta\sigma_{outer}$ and $\Delta\sigma_{inner}$ start to gradually increase in tension and compression, respectively, when the new tunnel face arrives approximately -2D away from the existing tunnel. Further advancement of the new tunnel continues to increase the stresses until the new tunnel face advances beyond 2.0D from the control section after which they taper off. Maximum tensile and compressive stresses of 1.0 MPa and 2.4 MPa, respectively, are developed on outer and inner sides of the invert section.

Fig. 6 shows complete profiles of $\Delta\sigma_{outer}$ and $\Delta\sigma_{inner}$ at the control section after completion of the new tunnel excavation. As shown, tensile stresses, as great as 1.0 MPa, are developed on the outer side of the crown and invert region, i.e., $-45° \leq \theta \leq 45°$ and $135° \leq \theta \leq 225°$, where θ is measured from the crown clockwise, while the compressive stresses are developed in the rest of the region. On the inner side, however, larger, but compressive, stresses, as great as 2.4 MPa, are developed in the region of $-45° \leq \theta \leq 45°$ and $135° \leq \theta \leq 225°$, while the rest of the region is subject to tensile stresses with a maximum of 1.8 MPa at the haunch area. The maximum tensile stress of 1.8 MPa in fact accounts for (36~90)% of the tensile strength of concrete $(2{\sim}5)$ MPa, which cannot be considered insignificant depending on existing stresses in the lining prior to the new tunnel excavation and the grade of concrete. Should the lining cracks due to the new tunnel construction, the likely location of crack formation would be the haunch area for the tunneling case considered.

4.2 Effect of plan crossing angle ($\boldsymbol{\theta_{xy}}$) - underpassing case

As underground subway networks become increasingly complex and congested, there are many situations where new tunnels are constructed to cross existing ones at various angles. In this section, the effect of plan crossing angle on the degree of interaction between the two tunnels is examined for the underpassing scenario.

The axial force and bending moment, and the associated normal stress profiles for the control section of the existing tunnel lining are shown for various plan crossing angles in Figs. 7-10. As can be seen in Fig. 7 for the axial force, the new tunnel construction induces tensile forces all around the lining irrespective of the plan crossing angle θ_{xy} with

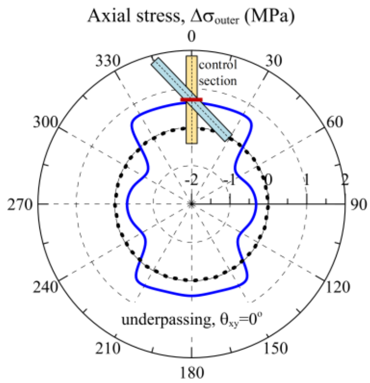

(a) $\theta_{xy} = 0°$

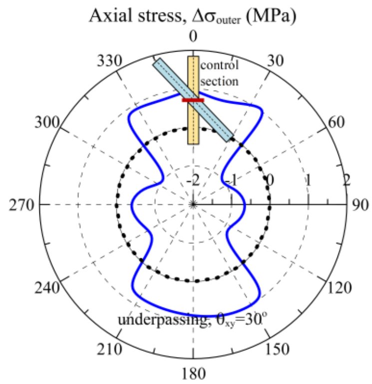

(b) $\theta_{xy} = 30°$

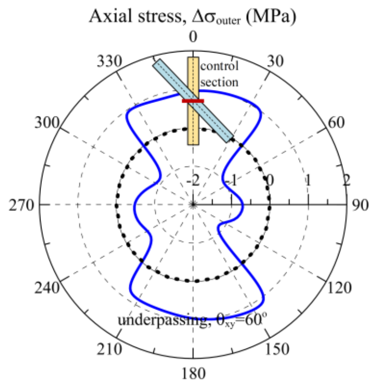

(c) $\theta_{xy} = 60°$

Fig. 9 Effect of plan crossing angle on new tunnel induced existing tunnel lining outer side normal stress (underpassing)

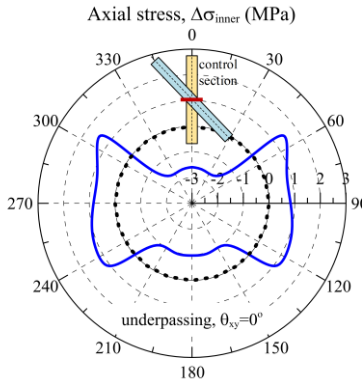

(a) $\theta_{xy} = 0°$

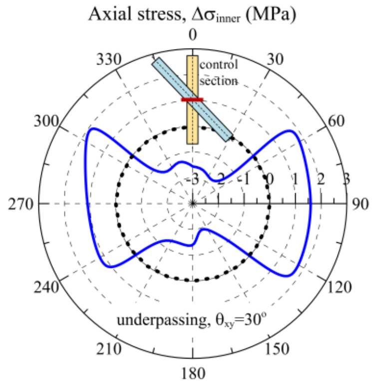

(b) $\theta_{xy} = 30°$

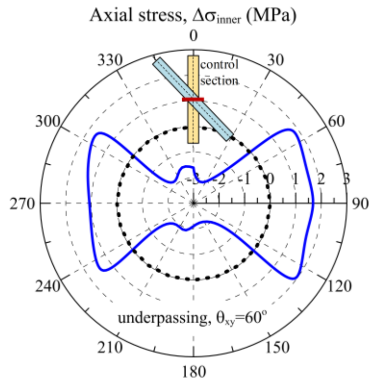

(c) $\theta_{xy} = 60°$

Fig. 10 Effect of plan crossing angle on new tunnel induced existing tunnel lining inner side normal stress (underpassing)

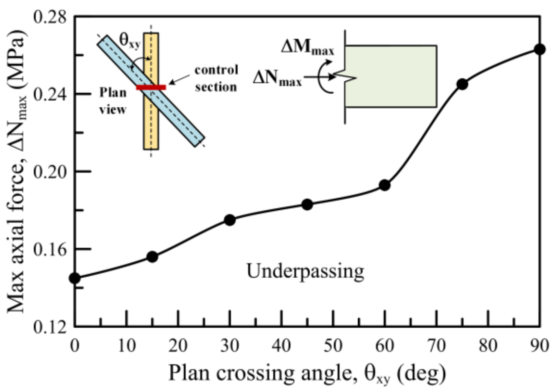

(a) Max. axial force (ΔN_{max})

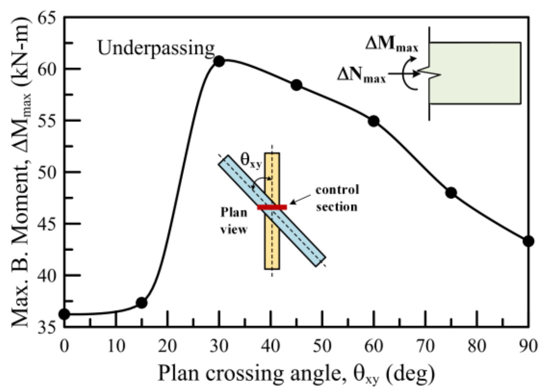

(b) Max. bending moment (ΔM_{max})

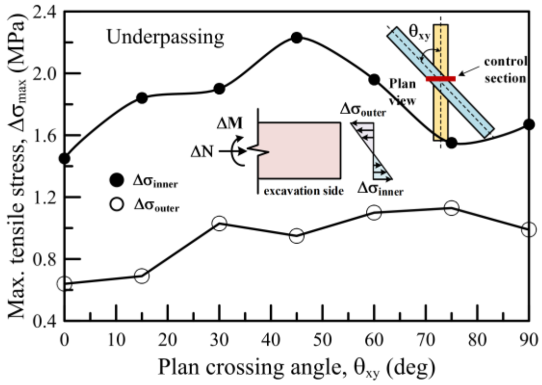

(c) Normal stresses ($\Delta\sigma_{outer}$, $\Delta\sigma_{inner}$)

Fig. 11 Variations of new tunnel induced maximum member forces and stresses with plan crossing angle (underpassing) maximum values ranging (0.13~0.24) MN. As expected, the magnitude and location of ΔN_{max} seem to change with the plan crossing angle. For example, the maximum axial force (ΔN_{max}) occurs at the invert for the overlapped ($\theta_{xy} = 0°$) and the 90° crossing ($\theta_{xy} = 90°$) cases while occurring in the region between the spring line and haunch areas for acute angles, i.e., $\theta_{xy} = (30\sim60)°$. Also shown is that, the maximum value of ΔN (ΔN_{max}) appears to increase as θ_{xy} increases with the largest ΔN_{max} of 0.24 MN occurring at $\theta_{xy} = 90°$. The bending moment profiles in Fig. 8, however, show that the maximum bending moment tends to occur at the spring line irrespective of the plan crossing angle with a tendency that larger ΔM_{max} develops when $\theta_{xy} = (30\sim60)°$ than the overlapped ($\theta_{xy} = 0°$) and the 90° crossing ($\theta_{xy} = 90°$) cases.

Shown in Figs. 9 and 10 are $\Delta\sigma_{outer}$ and $\Delta\sigma_{inner}$ profiles computed based on ΔN and ΔM for various plan crossing angles. As shown for $\Delta\sigma_{outer}$ in Fig. 9, the profile largely remains the same irrespective of θ_{xy}, showing that tensile stresses are developed in the region between shoulder and crown areas, i.e., $-30° \leq \theta \leq 30°$, with compressive stresses occurring elsewhere. An opposite trend is shown in the inner side normal stress $\Delta\sigma_{inner}$ profiles in Fig. 10 where it can be seen that tensile stresses are developed in the region between shoulder and haunch areas, i.e., $60° \leq \theta \leq 120°$. It is worth noting that the inner side tensile stresses of $\Delta\sigma_{inner} = (1.2\sim2.0)\ MPa$ are larger than those of the outer side $\Delta\sigma_{outer} = (0.4\sim1.0)\ MPa$, and that in both sides, larger tensile stresses are developed when constructing the new tunnel with acute plan crossing angles, i.e., $\theta_{xy} \approx (30\sim60)°$ than the overlapped (i.e., $\theta_{xy} = 0°$) and the 90° crossing (i.e., $\theta_{xy} = 90°$) cases. A critical zone in the existing tunnel lining for a given plan crossing angle would be the inner side between shoulder and haunch areas, i.e., $60° \leq \theta \leq 120°$ with a more unfavorable stress condition expected when constructing the new tunnel with acute plan crossing angles, i.e., $\theta_{xy} \approx (30\sim60)°$.

The results presented in Figs. 7-10 are compiled in Fig. 11 to show the variation of maximum member forces and sectional stresses with the plan crossing angle. As shown in Fig. 11(a), the maximum axial force (ΔN_{max}) gradually increases with θ_{xy} until θ_{xy} reaches 60° after which it rapidly increases to its maximum of $\Delta N_{max} = 0.25\ MN$ at $\theta_{xy} = 90°$. The maximum bending moment in Fig. 11(b), however, sharply increases with increasing θ_{xy} showing a peak value of $\Delta M_{max} = 60\ kN \cdot m$ at $\theta_{xy} = 30°$ and gradually decreases thereafter. The lining stresses due to the combined effects of ΔN and ΔM are shown in Fig. 11(c) with respect to the plan crossing angle θ_{xy}. As already observed in Figs. 9 and 10, the inner side maximum tensile stress is almost twice larger than that of the outer side for a given plan crossing angle. Also observed is that similar to the maximum bending moment plot, the maximum tensile stress becomes larger when excavating the new tunnel with acute plan crossing angle $\theta_{xy} = (30\sim60)°$ than with overlapped (i.e., $\theta_{xy} < 20°$) or near 90° plan crossing angle (i.e., $\theta_{xy} \approx 90°$). Greater impact on the existing tunnel should therefore be expected for cases with a plan crossing angle of $\theta_{xy} = (30\sim60)°$ than with near overlapped (i.e., $\theta_{xy} < 20°$) or near 90° plan crossing angle (i.e., $\theta_{xy} \approx 90°$) when a new tunnel is constructed under an existing tunnel.

In summary, the plan crossing angle significantly affects the degree of interaction between the new and the existing tunnel. More pronounced effect of new tunnel construction on the existing tunnel lining was observed for cases with acute plan cross angles in the range of $\theta_{xy} = (30\sim60)°$. The plan crossing angle θ_{xy} should be considered as a major influencing factor governing the new and existing tunnel interaction. Although these results need to be validated, localized stress concentration phenomenon when crossing with an acute angle may be responsible for such results.

4.3 Effect of vertical location of new tunnel with respect to existing tunnel

There are two possible new tunnel construction scenarios in terms of its vertical elevation relative to the existing tunnel, i.e., underpassing and overpassing cases. In order to investigate the relative impact of the new tunnel construction scenario on the existing tunnel, the underpassing and overpassing cases were examined for two plan crossing angle cases, i.e., $\theta_{xy} = 0°$ and 90°.

Figs. 12 and 13 show the progressive development of new tunnel construction induced lining member forces at the crown and invert of the control section for the underpassing cases. As shown in Fig. 12(a) for the overlapped ($\theta_{xy} = 0°$) case, the new tunnel construction mainly imposes tensile forces at both locations, but with much larger value at the invert of 0.14 MN than at the crown of 0.04 MN. In terms of the progressive development at the invert, the new tunnel advancement starts to impose additional axial force in the existing tunnel lining at a fairly constant rate when the new tunnel is at -2.0D away from the control section until it advances 2.5D from it. At the crown, on the other hand, the axial force seems to fluctuate between 0 and 0.04 MN during the new tunnel advancement. For the bending moment shown in Fig. 12(b), the increase in ΔM seems to be larger at the crown than at the invert despite the close proximity of the new tunnel to the invert, showing a maximum value of 20 kN-m and 8 kN-m, respectively, at the crown and invert. Similar to the axial force development, the new tunnel construction tends to add additional bending moment during the new tunnel advances in the region between -2.0D and 2.5D from the section.

The results in Fig. 12 indicate that for the overlapped underpassing cases, the crown area of the lining of the existing tunnel is subject to a large increase in bending moment while a large increase in axial force is likely at the invert. For a given section, most of increases in the member forces are found to occur during the new tunnel advancementinthe regionbetween-2.0D and 2.5D from the section. The 90° crossing case, i.e., $\theta_{xy} = 90°$, shows dramatically different results when compared to the

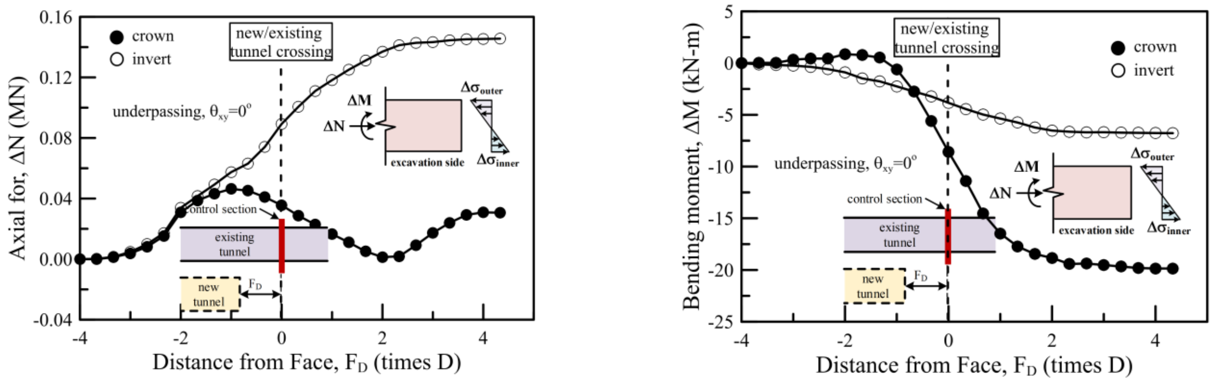

(a) Axial force (ΔN) (b) Bending moment (ΔM)

Fig. 12 Evolution of ΔN and ΔM with new tunnel advancement (underpassing, $\theta_{xy} = 0°$)

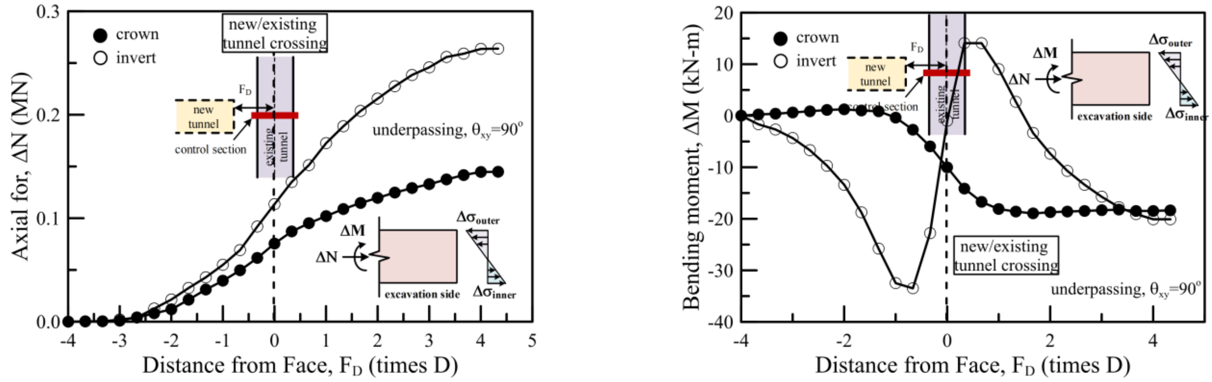

(a) Axial force (ΔN) (b) Bending moment (ΔM)

Fig. 13 Evolution of ΔN and ΔM with new tunnel advancement (underpassing, $\theta_{xy} = 90°$)

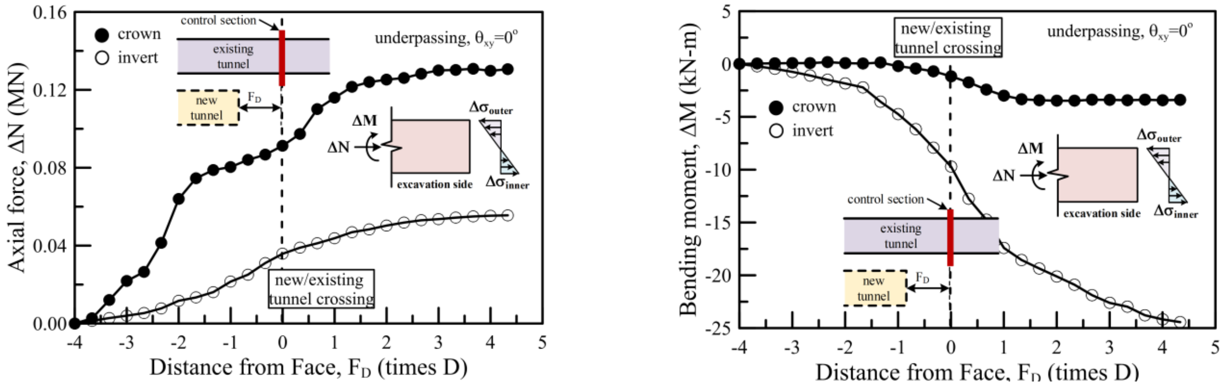

(a) Axial force (ΔN) (b) Bending moment (ΔM)

Fig. 14 Evolution of ΔN and ΔM with new tunnel advancement (overpassing with $\theta_{xy} = 0°$)

overlapped case ($\theta_{xy} = 0°$), the bending moment in particular, as shown in Fig. 13. Of salient feature is that the new tunnel construction induced axial forces at the crown and invert are twice larger than those of the overlapped case ($\theta_{xy} = 0°$) with a larger bending moment being developed at the invert than at the crown. Another of interest trend is that the maximum bending moment at the invert develops before the new tunnel passes the section, i.e., when the new tunnel face arrives at -0.8D from the section.

The new tunnel induced member forces for the overpassing cases are shown in Figs. 14 and 15, respectively, for $\theta_{xy} = 0°$ and 90°. As shown, unlike the underpassing cases, the overlapped case $\theta_{xy} = 0°$ yields twice larger maximum values, both in axial force and bending moment, than the 90° crossing case ($\theta_{xy} = 90°$), although the general trends are similar. Another of interest trend is that the location of the maximum member forces changes with the plan crossing angle. For example, the maximum axial force occurs at the crown when $\theta_{xy} = 0°$ while at invert when $\theta_{xy} = 90°$. The opposite is true for the bending moment as the maximums occur at the invert and at the crown, respectively, for $\theta_{xy} = 0°$ and $\theta_{xy} = 90°$. It can therefore be stated that when constructing a new tunnel above an existing one, the overlapped case imposes

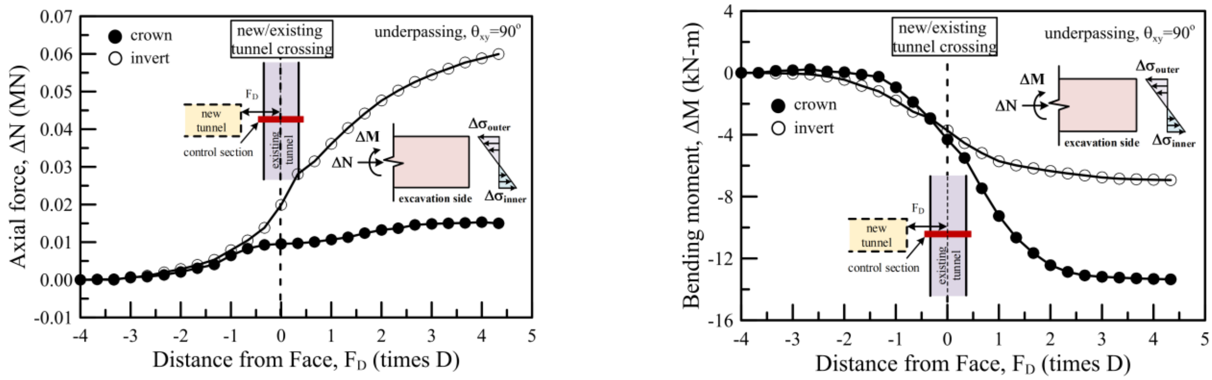

(a) Axial force (ΔN) (b) Bending moment (ΔM)

Fig. 15 Evolution of ΔN and ΔM with new tunnel advancement (overpassing with $\theta_{xy} = 90°$)

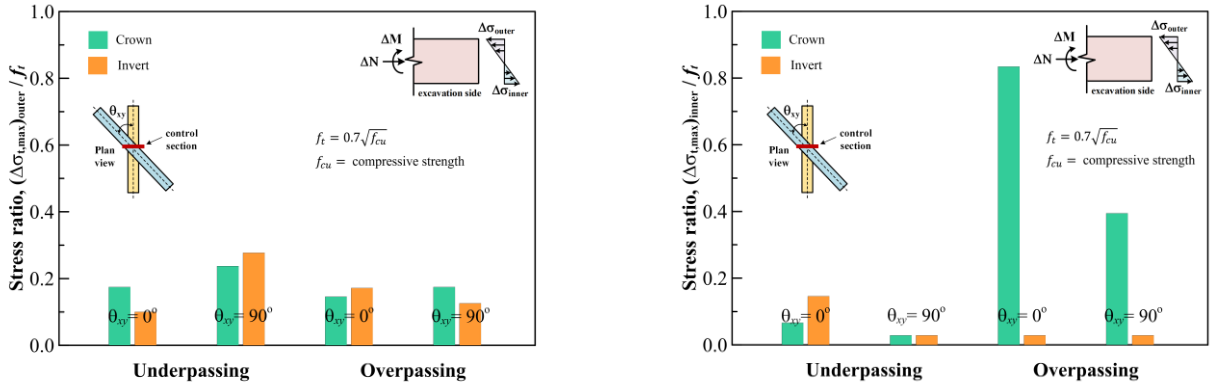

(a) Maximum stress-outer side ($\Delta\sigma_{outer}$) (b) Maximum stress-inner side ($\Delta\sigma_{inner}$)

Fig. 16 Variation of stress ratio with plan crossing angle (θ_{xy}) for underpassing and overpassing cases

greater additional member forces to the existing tunnel lining than the 90° crossing case.

A direct comparison between Fig. 12(b) and 14(b) allows to examine the effect of vertical location of the new tunnel relative to the existing tunnel on the existing lining. As shown, Fig. 12(b) indicates that the existing tunnel undergoes vertical compression for the case of underpassing as negative bending moments are developed at the crown. The overpassing case in Fig. 14(b), on the other hand, shows that the invert section is subject to negative bending moments, a sign of vertical elongation. These results are in line with those reported by Boonyarak and Ng (2015) and imply that the vertical location of a new tunnel has significant implication on the structural performance of existing lining.

The maximum lining tensile stress $\Delta\sigma_{t,max}$ at the crown and invert for the under- and overpassing cases are shown in Fig. 16 in a normalized fashion using the stress ratio, $SR = \frac{\Delta\sigma_{t,max}}{f_t}$, assuming the lining of M25 concrete, where $\Delta\sigma_{t,max}$ is computed maximum tensile stress increase and f_t is tensile strength of M25 concrete. Note that the tensile strength of M25 concrete was taken as $f_t = 0.3\sqrt{f_{cu}}$ where f_{cu} is the compressive strength, i.e., 25 MPa. These results, in fact, confirm the trends observed in Figs. 14 -15. For example, when considering maximum values, it is seen that that the 90° crossing case ($\theta_{xy} = 90°$) yields a 65% larger stress ratio of $SR = 0.28$ than the overlapped case ($\theta_{xy} = 0°$) of SR=0.17 when the new tunnel underpasses the existing tunnel. For the overpassing cases, on the other hand, the overlapped overpassing case yields a stress ratio (SR=0.83) at the crown which is twice larger than that (SR=0.39) of the 90° cross overpassing case, indicating that the overlapped excavation case is more critical than the crossing case when excavating a new tunnel above an existing tunnel.

Based on the limited cases considered, the new tunnel construction over an existing tunnel seems to have a greater impact on the existing tunnel lining than constructing it under the existing tunnel. The effect of plan crossing angle on the existing tunnel also varies with the vertical location of the new tunnel relative to the existing one such that the 90° crossing construction is more critical than the overlapped when underpassing. A reversed trend holds for which the new tunnel is constructed over the existing one. The results strongly suggest that the degree of impact of a new tunnel construction on an existing tunnel lining should be evaluated with due consideration of the vertical location of the new tunnel relative to the existing tunnel as well as the plan crossing angle.

5. Conclusions

This paper presents the results of a three-dimensional numerical investigation into the effect of new tunnel construction on an existing tunnel. A parametric study was conducted on a number of tunneling cases using a three-dimensional finite difference model with emphasis on the plan crossing angle of the new tunnel with respect to the existing tunnel axis, and the relative vertical position of the new tunnel with respect to the existing one. The following conclusions can be drawn at least for the tunneling cases considered in this study.

1) When a new tunnel is constructed under an existing tunnel, the new tunnel construction induces tensile forces all around the lining irrespective of the plan crossing angle θ_{xy} with the maximum axial force occurring at $\theta_{xy} = 90°$. The maximum bending moment, however, occurs at the spring line irrespective of the plan crossing angle with a tendency that it becomes larger when $\theta_{xy} = (30{\sim}60)°$. Corresponding tensile normal stresses developed in the existing tunnel lining also show similar trend of which larger tensile stresses are developed in the region between shoulder and haunch areas when the new tunnel is constructed with plan crossing angles ranging $\theta_{xy} = (30{\sim}60)°$. The new tunnel induced lining member forces and stresses for a given section are mainly developed during the new tunnel advancement of the region between -2.0D and 2.5D from the section regardless of the plan crossing angle. Should a mitigation measure be implemented to a section in an existing tunnel, it needs to be executed before the new tunnel face enters the influence zone, i.e., the region between -2.0D and 2.5D from the section.

2) The limited cases analyzed for the new tunnel construction scenario of overpassing the existing tunnel indicate that the overlapped case, i.e., $\theta_{xy} = 0°$, imposes greater member forces to the existing tunnel lining than the crossing case, i.e., $\theta_{xy} = 90°$. A reversed trend holds for the underpassing construction scenario. A direct comparison between the underpassing and overpassing construction scenarios suggests that the impact of the new tunnel construction becomes greatest when the new tunnel is crossing at $\theta_{xy} = 90°$ above the existing tunnel, suggesting that the overpassing new tunnel construction scenario is more critical than the underpassing in view of the existing tunnel lining stability.

3) Although limited, the findings from this study suggest that the effect of new tunnel construction on the existing tunnel lining is greatly affected not only by the plan crossing angle but by the relative vertical location of the new tunnel with respect to the existing tunnel. The level of impact of a new tunnel construction on an existing tunnel lining should therefore be evaluated with due consideration of the vertical location of the new tunnel relative to the existing tunnel as well as the plan crossing angle.

4) The numerical model adopted in this study has not been validated as fully instrumented field tunneling cases are not readily available. As part of continuing research in a future study, the numerical model will be validated against instrumented results from model tests and/or field tunneling cases.

Acknowledgments

This research was supported by National Research Foundation of Korea (Project Number: NRF-2017R1E1A1A01077246). The financial support is gratefully acknowledged.

References

Boonyarak, T. and Ng, C.W.W. (2015), "Effects of construction sequence and cover depth on crossing-tunnel interaction", *Can. Geotech. J.*, **52**(7), 851-867. https://doi.org/10.1139/cgj-2014-0235.

Byun, G.W., Kim, D.G. and Lee, S.D. (2006), "Behavior of the ground in rectangularly crossed area due to tunnel excavation under the existing tunnel", *Tunn. Undergr. Sp. Technol.*, **21**(3), 361-361. https://doi.org/10.1016/j.tust.2005.12.178.

Choi, J.I. and Lee, S.W. (2010), "Influence of existing tunnel on mechanical behavior of new tunnel", *KSCE J. Civ. Eng.*, **14**(5), 773-783. https://doi.org/10.1007/s12205-010-1013-8.

Cooper, M.L., Chapman, D.N. and Rogers, C.D.F. (2002), "Prediction of settlement in existing tunnel caused by the second of twin tunnels", *Transport. Res. Rec.*, **1814**(1), 103-111.

Davis, E.H. (1968), *Theories of Plasticity and the Failure of Soil Masses*, in *Soil Mechanics: Selected topics*, Butterworth's London, U.K. 341-380.

Djelloul, C., Karech, T., Demagh, R., Limam, O. and Martinez, J. (2018), "2D numerical investigation of twin tunnels-Influence of excavation phase shift", *Geomech. Eng.*, **16**(3), 295-308. https://doi.org/10.12989/gae.2018.16.3.295.

Eskandari, F., Goharrizi, K.G. and Hooti A. (2018), "The impact of EPB pressure on surface settlement and face displacement in intersection of triple tunnels at Mashhad metro", *Geomech. Eng.*, **15**(2), 769-774. https://doi.org/10.12989/gae.2018.15.2.769.

Hansmire, W.H., Romero, V.S. and McRae, M.T. (2017), "Multiple tunnels in soil with shotcrete linings on Tren Urbano, San Juan, Puerto Rico", *Proceedings of the 5th International Conference on Case Histories in Geotechnical Engineering*, New York, U.S.A., April.

Itasca Consulting Group, Inc. (2017), *FLAC3D — Fast Lagrangian Analysis of Continua in Three-Dimensions*, Ver. 6.0, Itasca, New York, U.S.A.

Lai, J., Fan, H., Chen, J., Qui, J. and Wang, K. (2015), "Blasting vibration monitoring of undercrossing railway tunnel using wireless sensor network", *Int. J. Distrib. Sens. N.*, **11**(6), 703980. https://doi.org/10.1155/2015/703980.

Nawel, B. and Salah, M. (2015), "Numerical modeling of two parallel tunnels interaction using three-dimensional Finite Elements Method", *Geomech. Eng.*, **9**(6), 775-791. https://doi.org/10.12989/gae.2015.9.6.775.

Ng, C.W.W., Shi, J. and Hong, Y. (2013), "Three-dimensional centrifuge modelling of basement excavation effects on an existing tunnel in dry sand", *Can. Geotech. J.*, **50**(8), 874-888. https://doi.org/10.1139/cgj-2012-0423.

Queiroz, P.I.B., Roure, R.N. and Negro, A. (2006), "Bayesian updating of tunnel performance for K_o estimate of Santiago gravel", *Proceedings of the International Symposium on Geotechnical Aspects of Underground Construction in Soft Ground*, London, U.K., June.

Talebinejad, A., Chakeri, H. and Moosavi, M. (2013), "Investigation of surface and subsurface displacements due to multiple tunnels excavation in urban area", *Arab. J. Geosci.*, **7**(9), 3913-3923. https://doi.org/10.1007/s12517-013-1056-5.

Waltham, A.C. (1994), *Foundations of Engineering Geology*, Blackie Academic & Professional, London, U.K.

Yoo, C. and Song, A.R. (2006), "Effects of tunnel construction on an existing tunnel lining", *J. Kor. Tunn. Undergr. Sp. Assoc.*, **8**(4), 307-324.

Zhang, Z. and Huang, M. (2014). "Geotechnical influence on existing subway tunnels induced by multiline tunneling in Shanghai soft soil", *Comput. Geotech.*, **56**(3), 121-132. https://doi.org/10.1016/j.compgeo.2013.11.008.

Zhang, M., Fan, J. and Pan, B. (2015), "Analysis on construction influence of the underpass of oblique crossing subway tunnel", *Appl. Mech. Mater.*, **716-717**, 418-423. https://doi.org/10.4028/www.scientific.net/AMM.716-717.418.

IC